Published in final edited form as:
*Cancer Res*. 2014 April 15; 74(8): 2295–2305. doi:10.1158/0008-5472.CAN-13-1803.

# IGF-I regulates redox status in breast cancer cells by activating the amino acid transport molecule xC⁻

**Yuzhe Yang**[1,2] and **Douglas Yee**[1,2,3]

[1]Masonic Cancer Center, University of Minnesota, Minneapolis, Minnesota

[2]Department of Pharmacology, University of Minnesota, Minneapolis, Minnesota

[3]Department of Medicine, University of Minnesota, Minneapolis, Minnesota

## Abstract

Insulin-like growth factors (IGFs) stimulate cell growth in part by increasing amino acid uptake. xCT (*SLC7A11*) encodes the functional subunit of the cell surface transport system xC⁻ which mediates cystine uptake, a pivotal step in glutathione synthesis and cellular redox control. In this study, we show that IGF-I regulates cystine uptake and cellular redox status by activating the expression and function of xCT in estrogen receptor-positive (ER+) breast cancer cells by a mechanism that relies on the IGF receptor substrate-1 (IRS-1). Breast cancer cell proliferation mediated by IGF-I was suppressed by attenuating xCT expression or blocking xCT activity with the pharmacological inhibitor sulfasalazine (SASP). Notably, SASP sensitized breast cancer cells to inhibitors of the IGF-I receptor in a manner reversed by the ROS scavenger N-acetyl-L-cysteine. Thus, IGF-I promoted the proliferation of ER+ breast cancer cells by regulating xC⁻ transporter function to protect cancer cells from ROS in an IRS-1 dependent manner. Our findings suggest that inhibiting xC⁻ transporter function may synergize with modalities that target the IGF-I receptor to heighten their therapeutic effects.

### Keywords

Insulin-like growth factor 1 receptor; insulin receptor substrate 1; xC⁻ transporter; reactive oxygen species; breast cancer

## Introduction

The insulin like growth factor (IGF) signaling pathway stimulates growth and metastasis in many types of cancer (1, 2). Ligand dependent activation of the type I IGF receptor (IGF-IR) results in recruitment of the insulin receptor substrate (IRS) adaptor molecules to transduce signals to downstream signaling cascades and ultimately regulate cell behavior. In breast cancer cells, IRS-1 and IRS-2 are the two primary adaptor proteins that regulate IGF-IR

Correspondence to Dr. Douglas Yee, Masonic Cancer Center, University of Minnesota, MMC 806, 420 Delaware St. SE, Minneapolis, 55455. Phone: 612-626-8487; Fax: 612-626-3069; yeexx006@umn.edu.

The authors declare no conflict of interest.

signaling (3). In model systems, IRS-1 mainly promotes cell proliferation (4, 5), while IRS-2 stimulates cell motility (5, 6).

The clinical results of anti-IGF-IR monoclonal antibody trials in breast cancer have been disappointing (7). Given that breast cancer is highly heterogeneous, there is an urgent need to identify predictive biomarkers (8, 9) that correlate with IGF-IR driven tumors and to characterize additional molecular targets that may synergize with anti-IGF-IR therapy. To identify potential biomarkers, our laboratory characterized the gene expression profiles of T47D variant cell lines with differential IRS protein expression (5) upon IGF-I stimulation (Becker *et al*, submitted). *SLC7A11* mRNA expression was upregulated by IGF-I in an IRS-1 specific manner.

*SLC7A11* (or xCT) encodes the functional subunit of cystine-glutamate exchange transporter: $xC^-$. $xC^-$ transporter mediates the uptake of extracellular L-cystine in exchange for L-glutamate. The cell membrane expression of $xC^-$ transporter is essential for uptake of extracellular cystine to generate intracellular cysteine to maintain intracellular glutathione (GSH) levels (10). GSH controls the intracellular redox state (10, 11) protecting cells from multiple sources of damage including chemical, radiological, and direct reactive oxygen species (ROS) (12) mediated damage. The roles of ROS in cancer are complex due to the heterogeneity of downstream signaling cascades activated in response to their generation (13, 14). Continuous exposure to endogenous or exogenous ROS stress results in some cancer cells undergoing apoptosis or growth arrest (15). Other cells can develop redox adaptive mechanisms (16) to prevent apoptosis and also increase genomic instability (17), promote malignant transformation, metastasis (18), and contribute to drug resistance (19). Recent studies reported that xCT deficiency sensitizes malignant cells' response to oxidative stress (15, 20) and inhibits cancer cell growth (10) and metastasis (21). The expression level of xCT predicts chemosensitivity to multiple drugs (22), and combining the xCT chemical inhibitor sulfasalazine (SASP) with a HSP90 inhibitor celastrol shows synergistic anti-cancer effects (23).

This study determined the role for IGF-I stimulation of breast cancer cells in the generation of intracellular ROS through the regulation of xCT expression and function. Co-targeting $xC^-$ transporter with anti-IGF-IR therapy was explored as a way to increase the efficacy of targeting both pathways. We found that IGF-I stimulated $xC^-$ expression in an IRS-1 dependent manner. IGF-I also regulated cellular redox status partially through $xC^-$ transporter and thereby enhancing cancer cell proliferation.

## Materials and Methods

### Reagents and antibodies

Growth media and supplements were purchased from Invitrogen (Grand Island, NY). IGF-I was purchased from GroPep (Adelaide, Australia). IGF-II was purchased from Gemini (Woodland, CA). Sulfasalazine (≥98%), L-Buthionine-sulfoximine (≥97%), N-Acetyl-L-cysteine, LY294002, U0126, and actin antibody were purchased from Sigma-Aldrich (St. Louis, MO). Humanized anti-IGF-IR monoclonal antibody huEM164 was generously provided by Immunogen Inc. (Norwood, MA). Antibodies for phosphorylated AKT serine

473, total and phospho-IGF-IR, total and phospho-phosphorylated p44/42 (MAPK), phospho-p38$^{MAPK}$, and IRS-1 were purchased from Cell Signaling Technology (Beverly, MA). The IRS-2 antibody was purchased from Santa Cruz Biotechnology (Santa Cruz, CA). The xCT antibody for Western blot analysis was purchased from Novus Biologicals (Littleton, CO). Horseradish peroxidase-conjugated anti-phosphotyrosine (PY-20) was purchased from BD Biosciences (San Jose, CA). Anti-rabbit and anti-mouse horseradish peroxidase-conjugated secondary antibodies were purchased from Pierce (Rockford, IL). 5-(and-6)-carboxy-2′,7′-dichlorofluorescein diacetate was purchased from Invitrogen (Carlsbad, CA).

### Cell lines and culture

MCF-7, ZR-75-1, T47D, MDA-MB-231, BT549, and HS578T cells were purchased from the ATCC (Manassas, VA) and cultured following ATCC's instruction. MCF-7L cells were kindly provided by C. Kent Osborne (Baylor College of Medicine) and maintained in improved MEM Richter's modification medium (zinc option) supplemented with 5% FBS and 11.25 nmol/L insulin. MCF-7L were evaluated by comparative genomic hybridization (data not shown) and found to be nearly identical to the MCF-7 cells distributed by the ATCC. MCF-7 TamR cells were generated as described (24). T47D-YA-IRS-1 and T47D-YA-IRS-2 were maintained in Eagle's Minimal Essential Medium supplemented with 5% fetal bovine serum, 11.25 nmol/L insulin, 10 ml/L 100X non-essential amino acids, 200 μg/ml of G418, and 200 μg/ml of hygromycin. All cells were grown at 37 °C in a humidified atmosphere containing 5% $CO_2$.

### Immunoblot

Cells were plated at a density of $3 \times 10^5$ in 60-mm-diameter. Upon reaching 80% confluency, cells were switched to serum-free medium (SFM) for 24 hour to synchronize cell status, after which treatments were added. Treated cells were washed twice with ice-cold phosphate buffered saline (PBS) on ice and lysed with lysis buffer of 50 mM Tris-Cl (pH 7.4), 1% Nonidet P-40, 2 mM EDTA (pH 8.0), 100 mM NaCl, 10 mM sodium orthovanadate, 1 mM phenylmethysulforny fluoride, and with proteases inhibitor cocktails. Lysates were centrifuged at 21,000 rpm for 15 minutes at 4 °C. Protein concentrations were measured using the bicinchoninic acid protein assay reagent kit (Pierce). Cellular protein (80 μg) was resuspended in 5x Laemmli loading buffer with 60 mg/ml DTT and was resolved by SDS-PAGE, transferred to nitrocellulose membrane, and immunoblotted according to manufacturer guidelines.

### siRNA transfection and cell stimulation

Cells were cultured in growth medium to reach confluency of 80% then were transfected with 30 nmol/L siRNA (siRNAs SMARTpool were purchased from Santa Cruz Biotechnology) using the TransIT-siQUEST transfection reagent (Mirus, Madison, WI) according to the manufacturer's protocol. 48 hours later, cells were washed twice with PBS and serum starved for another 24 hours in SFM followed by treatments as indicated in the figure legends.

### Stable xCT down-regulation with shRNA

Lentiviral pKLO.1 vectors encoding a xCT mRNA specific shRNA sequence (CCGGGCTGATTTATCTTCGATACAACTCGAGTTGTATCGAAGATAAATCAGCTTTTTG) or a scrambled shRNA were purchased from BioMedical Genomics Center (University of Minnesota) and were introduced to MCF-7 cells. 8 mg/ml polybrene was added to increase infection efficiency. MCF-7 cells infected with shRNA were maintained by 1 μg/ml puromycin selection pressure.

### Reverse transcription-quantitative real-time polymerase chain reaction

Cells were plated at a density of $2 \times 10^5$ in 6-well-plates in growth media to reach 80% confluency then synchronized in SFM for 24 hours followed by treatments indicated in the figure legends. Cellular RNA was isolated using TriPure Reagent according to the manufacturer (Roche, Belgium). For quality control and to determine concentration, a 260:280 ratio assay was conducted on a spectrophotometer. Forward and reverse primers were designed to target the following transcripts: *SLC7A11* (xCT) 5′-GGCAACCGCGTAATACTTG-3′ and 5′-TTGCAAGCTCACAGCAATTC-3′; *IRS-1* 5′-TCACAGCAGAATGAAGACC-3′ and 5′-CTACTGATGAGGAAGATATGAGG-3′; *IRS-2* 5′-TCGTGAAAGAGTGAAGATCTG-3′ and 5′-TCCAAACACAGTCATTGCT-3′; *CD44v* 5′-AGAAGGTGTGGGCAGAAGAA-3′ and 5′-AAATGCACCATTTCCTGAGA-3′; and *RPLPO* 5′-TGCTGATGGGCAAGAACAC-3′ and 5′-GAACACAAAGCCCACATTCC-3′ A total of 1 μg of RNA was reverse transcribed using the Transcriptor Reverse Transcriptase Kit, and quantitative PCR was conducted using the Universal SYBR Green Kit according to the manufacturer's protocol (Roche) on an Eppendorf (Hamburg, Germany) Mastercycler Realplex$^4$ machine. The relative concentration of mRNA was calculated using cycle threshold values that were derived from a standard curve and normalized to ribosomal protein, large, Po (RPLPO) as an internal control.

### Monolayer growth assay

Cells were plated in 24-well-plates at a density of 15,000 cells per well, allowed to attach overnight and starved in SFM for 24 hours to synchronize cells. After 5 days of treatments, growth was assessed via the 3-(4,5-dimethylthiazol-2-yl)-2,5-diphenyltetrazolium bromide (MTT) assay. 50 μl of 5 mg/ml MTT solution in SFM were added to each well and incubated for 4 hours at 37 °C. Media were aspirated and formazan crystals were lysed with 500 μl of solubilization solution (95% dimethylsulfoxide + 5% improved minimal essential media). Absorbance was measured with a plate reader at 570 nm using a 650 nm differential filter to assess growth.

### Anchorage-independent growth

A 1 ml layer of 1% Seaplaque-agarose (BioWhittaker, Rockland, ME) in 1.5% FBS-containing growth media was solidified into each well of a 6-well plate. The bottom layer was overlaid with 1 ml of a 1% top agar mixture for 12,000 cells per well with indicated treatments. All plates were incubated at 37 °C for 14 days. Colonies was counted on a light

microscope with an ocular grid. Five random fields were counted per well and only colonies exceeding half of a grid square were scored.

### Radiation delivery

A dosage from 1~10 Gray was delivered to cell cultures by X-RAD 320 Biological Irradiator (Precision X-ray, North Branford, CT). Beam hardening filter= 2mm Al, dose rate: 3 Gy/min at 320 kV, 12.5 mA, 50 cm SSD.

### Glutathione measurement

Cells were plated at a density of 10,000 in 96-well clear bottom white plates, allowed to equilibrate overnight, and starved in SFM for 24 hours followed by treatments. Intracellular reduced glutathione concentrations were measured by using GSH/GSSG-Glo™ Assay following manufacturer's instruction (Promega, Madison, WI). Readings were further normalized to CellTiter-Glo® Luminescent Cell Viability Assay following the manufacturer's guideline (Promega).

### Glutamic acid assay

Cells were plated at a density of 20,000 in 24-well plates, allowed to equilibrate overnight, and starved in SFM for 24 hours followed by treatments. Glutamic acid level in extracellular media was determined by Amplex® Red Glutamic Acid/Glutamate Oxidase Assay Kit according to manufacturer's protocol (Invitrogen, Carlsbad, CA). The glutamic acid readings were further normalized to CellTiter-Glo® Luminescent Cell Viability Assay following the manufacturer's guideline (Promega).

### Reactive oxygen species assay

Cells were seeded at a density of 10,000 in 96-well clear bottom black plates, allowed to equilibrate overnight, and starved in SFM for 24 hours followed by treatments. Intracelluar ROS levels were determined by using OxiSelect™ Intracellular ROS Assay Kit according to manufacturer's guideline (Cell Biolabs, Inc., San Diego, CA)

### Cell cycle analysis

Cells were typsinized, washed twice in ice-cold PBS, and fixed in 70% ice-cold ethanol −20 °C over night. Cell cycle analyses were performed on propidium iodide-stained nuclei by using a FACSCalibur flow cytometer (Becton-Dickinson Biosciences, Heidelberg, Germany). Single cells were gated, 10,000 events were collected and analyzed by FlowJo (Tree Star Inc., Ashland, OR) software.

### Clinical data set analysis

The relative mRNA expression of *xCT* in human breast tumor samples was determined by searching the Oncomine database (version 4.4.3, September 2012 data release (25). *xCT* mRNA expression was queried in TCGA breast dataset using reporter A_32_P165472. For prognostic analyses, overall survival and distant metastasis-free survival, stratified by expression (all percentiles between the lower and upper quartiles were computed, and the

best performing threshold was used as a cutoff) of the gene of interest (*xCT*: 207528_s_at), were presented as Kaplan-Meier plots and tested for significance using log-rank tests.

### Statistical analysis

All data except clinical data sets were analyzed with the unpaired Student's t test with the use of Excel 2008 (Microsoft, Redmond, WA). A p value of $<0.05$ was considered statistically significant (* or # $p<0.5$, ** or ## $p<0.01$, *** or ### $p<0.001$).

## Results

### IGF-I stimulated SCL7A11 (xCT) mRNA expression in an IRS-1 dependent manner in estrogen receptor positive luminal but not in basal-like breast cancer cells

T47D-YA cells express neither IRS-1 nor IRS-2 (12). We created T47D-YA cells that stably expressed either IRS-1 or IRS-2 cDNA (5). T47D-YA, T47D-YA IRS-1 expressing cells (T47D-YA-IRS-1), and T47D-YA IRS-2 expressing cells (T47D-YA-IRS-2) were used to generate IRS isoform specific gene profiling upon IGF-I stimulation (Becker *et al*, submitted). *SLC7A11* (xCT) was one of the genes regulated by IGF-I only in T47D-YA-IRS-1 cells. To confirm the gene array result, quantitative reverse transcript PCR was performed using primers specific to xCT. The result was consistent with gene array data, after 4 hours of IGF-I exposure, xCT mRNA expression was significantly induced only in the T47D-YA-IRS-1 cells (Figure 1A).

We next examined the mRNA expression of xCT upon IGF-I stimulation in two classes of human breast cancer cells: three estrogen receptor (ER) positive breast cancer cell lines: MCF-7, T47D, and ZR-75-1, where IRS-1 mRNA expression was higher than in the three ER-negative breast cancer cell lines: MDA-MB-231, BT549, and HS578T, where IRS-2 was the predominant isoform expressed (Figure 1B left panel). IRS-1 and -2 protein expression was examined in four of the cell lines (Figure 1C) to confirm the mRNA expression levels. In the three ER positive cell lines, xCT mRNA expression was significantly upregulated by IGF-I, while no regulation was observed in the ER-negative cells (Figure 1B right panel) although the basal expression of xCT mRNA was significantly higher. Since ER regulates IRS-1 expression (26), we further investigated regulation of xCT in MCF-7L cells and MCF-7L selected for resistance to tamoxifen (TamR) cells as previously described (24). TamR cells expressed lower levels of IRS-1 (Figure 1D left panels) and IGF-IR while maintaining insulin receptor levels (24). IGF-I treatment stimulated xCT mRNA and protein expression in MCF-7L parental cells but not in the MCF-7L TamR cells. In parental cells, IGF-II and insulin induced xCT mRNA and protein expression while in TamR cells none of the ligands stimulated expression of xCT (Figure 1D right panels) above their higher basal levels. This suggested that without sufficient IRS-1 expression there is little effect on xCT expression despite functional insulin receptor signaling.

To evaluate the relevance of xCT expression in human primary breast cancers, we evaluated its expression in The Cancer Genome Atlas (TCGA) database. We found that the xCT relative mRNA expression in invasive ductal breast cancer (IDBC) samples was significantly higher than that in normal breast tissue. ER positive IDBC expressed lower

levels of xCT gene compared to ER negative or triple negative IDBC (Figure 2A). We next utilized a large public microarray database to evaluate the prognostic relevance of xCT in breast cancer patients (27). We found that high xCT expression significantly correlated with poor overall survival (OS) and distant metastasis free survival (DMFS) in estrogen receptor positive patients (Figure 2B). These findings from primary breast cancer specimens were consistent with our laboratory observations. The results implied that xCT expression and function might link to outcome and expression levels varied among the intrinsic subtypes of breast cancer.

To further confirm the role of IRS-1 in IGF-I regulation of xCT expression, either control or IRS-1 specific siRNAs (Figure S1) were transfected into ER positive cells (Figure 3A upper panels, S2 A). xCT mRNA expression and protein expression in MCF-7, T47D, and ZR-75-1 were induced by IGF-I only when IRS-1 was expressed at normal levels (Figure 3A lower panels, S2 B). Expression of xCT protein was seen after 24 hour of IGF-I stimulation likely due to a requirement for protein synthesis. These results suggested that IGF-I stimulated xCT expression in an IRS-1 dependent manner in ER positive breast cancer cells.

We next evaluated potential downstream signaling pathway required for IGF-I regulated xCT expression. We treated MCF-7 cells with anti-IGF-IR monoclonal antibody, huEM164, IGF-IR/insulin receptor tyrosine kinase inhibitor AEW-541, PI3K pathway inhibitor LY294002, or MEK inhibitor U01026 (Figure 3B, S3). IGF-I regulated xCT mRNA expression via IGF-IR was dependent on PI3K pathway signaling but not MAPK.

### IGF-I stimulated $xC^-$ transporter function

To investigate whether $xC^-$ function was affected by IGF-I stimulation, we performed two direct functional assays to measure the intracellular level of reduced GSH and the extracellular level of glutamic acid in three ER positive breast cancer cell lines and MDA-MB-231 cells. After 24 hours of IGF-I exposure, significant induction of both extracellular glutamic acid levels and intracellular reduced GSH concentrations in MCF-7 and T47D cells was observed but not in MDA-MB-231 (Figure 4A, 4B; reduced GSH data for MDA-MB-231 not shown).

To demonstrate that these effects were mediated by xCT, we used sulfasalzasine (SASP) an inhibitor of $xC^-$ function. Cells treated with 0.1 mM SASP (Figure S4 A, B) (10, 15, 23), showed depletion of intracellular GSH and diminished IGF-I regulated GSH levels (Figure 4B). GSH production requires gamma-glutamylcysteine synthetase function to ligate cysteine with glutamate. Buthionine sulfoximine (BSO) (28) inhibits this ligation and Figure 4B shows BSO had similar effects to SASP. Taken together, these data show that IGF-I regulation of $xC^-$ transporter function results in the import of cystine to increase the intracellular reduced GSH levels via an IRS-1 dependent manner in ER positive breast cancer cells. In the ER-negative breast cancer cell line, MDA-MB-231, high basal extracellular levels of glutamic acid were consistent with the expression of xCT in ER-negative primary breast cancers (Figure 2A).

### IGF-I regulated cellular redox status via xC⁻ transporter

Reduced GSH is a major cellular antioxidant molecule controlling cellular redox balance. We next examined whether IGF-I induced intracellular GSH level might further regulate cellular ROS level in cancer cells. We either irradiated (29) or treated cells with mitomycin C to induce intracellular ROS production. A ROS-sensitive fluorescent probe 2′,7′-dichlorofluorescein diacetate (DCFH-DA) was used to detect cellular ROS. 10 gray irradiation (Figure S5 A) or 0.1 μg/ml mitomycin C (Figure S5 B) significantly increased the intracellular ROS levels. The irradiation induced ROS was reduced by treating cells with ROS scavenger N-acetyl cysteine (NAC) (30) (Figure 5C right panel, S4E right panel). A ROS insensitive probe 5-(and-6)-carboxy-2′,7′-dichlorofluorescein diacetate (carboxy-DCFDA) was used as assay control (Figure 5C right panel). IGF-I treatment blunted the response to ROS production in MCF-7 and T47D (Figure 5A, S5 A, B) but not in the basal-like MDA-MB-231 cells (Figure S5 A). The IGF-I-mediated reduction of ROS was diminished (Figure 5A, S5 A) or partially attenuated (Figure 4A right panel, S5 B) when cells had been pretreated with 0.1 mM SASP. Since xCT expression and function were higher in basal like breast cancer cells (Figure 1B right panel, 2A, 4A) than in ER positive MCF-7 cells, the basal ROS levels in MDA-MB-231 cells were lower than in MCF-7 (Figure S5 A).

IGF-I treatment markedly reduced the phosphorylated form of $p38^{MAPK}$, a major effecter of ROS (13, 31), in MCF-7 and T47D cells. Consistent with the results obtained from direct ROS measurement experiments, pretreatment of ER positive cells with SASP, attenuated phosphorylation of $p38^{MAPK}$ after IGF-I treatment (Figure 5B, S5B).

Thus, our results suggested that IGF-I reduced cellular redox level specifically, but not completely, by stimulating the expression and function of xC⁻ transporter in ER positive breast cancer cells. We also found that IGF-I-induced ROS reduction was mediated by the IGF-IR/PI3K signaling axis as pathway inhibitors (huEM164, LY 294002, and AEW-541) decreased IGF-I's ability to reduce ROS generation (Figure 5C left panel).

In addition to the findings above, anchorage independent growth assays showed that SASP significantly sensitized MCF-7 cells response to both irradiation and mitomycin C treatments in serum depleting condition, which was reversed by treating cells with NAC (Figure 5D). We further verified that BSO had similar effects as SASP did (Figure S8A), which was partially reversed by adding NAC. Our data implied that SASP could enhance response to ROS inducing therapies by lowering intracellular GSH level.

### Disruption xC⁻ transporter function suppressed IGF-I-induced monolayer and anchorage independent growth

Increased ROS levels have been reported to arrest growth or even cause apoptosis in cancer cells which lack oxidative adaptive mechanisms (13). MCF-7 cells have relatively high basal levels of ROS under serum depleting condition (Figure S5 A), which resulted in partial growth arrest (Figure 6A, B, Table 1). IGF-I induced MCF-7 cell proliferation might be mediated by stimulating xC⁻ transporter function to increase cellular GSH level to protect cells from ROS. To test this hypothesis, we either pretreated MCF-7 cells with SASP to

disrupt $xC^-$ transporter function or stably infected xCT-specific shRNA (Figure S6) to downregulate its expression level and performed monolayer growth assays. We found that 0.1 mM SASP inhibited the function of $xC^-$ transporter without significant cytotoxicity in MCF-7 (Figure S4 A). Both chemical inhibition and genetic downregulation of xCT expression significantly suppressed IGF-I-induced monolayer growth (Figure 6A, 6B). SASP effects were reversed by adding NAC (Figure 6A). Cell cycle flow cytometry analysis showed that IGF-I stimulated cell S phase frequency was partially repressed when $xC^-$ transport was disrupted, which could be rescued by NAC (Table 1). Anchorage independent growth assays in MCF-7 cells showed similar results (Figure 6C). Parallel sets of experiments were done by treating cells with BSO instead of SASP to directly investigate the involvement of cellular GSH in these observations (Figure S8 B, C) with similar results. These data indicated that IGF-I stimulates MCF-7 cell growth partially by regulation of $xC^-$ transporters to control cellular GSH and redox levels.

### Disruption of $xC^-$ transporter sensitized ER positive breast cancer cells to anti-IGF-IR therapy

SASP treated MCF-7 cells showed significant intracellular GSH depletion resulting in elevated ROS and phospho-$p38^{MAPK}$ (Figure 5 A-C). Anti-IGF-IR therapy such as huEM164 and AEW-541 both diminished IGF-I regulation of cellular ROS (Figure 5C) and $p38^{MAPK}$ activation (Figure S3) while increasing the basal $p38^{MAPK}$ activity in MCF-7 cells (Figure S3). Thus, combining anti-IGF-IR drugs with the xCT inhibition might be combined to improve growth suppression.

In anchorage independent growth assays, we treated MCF-7 cells with 1 μg/ml huEM164 or 0.1 μM AEW-541. These lower drug doses were unable to sufficiently suppress IGF-I stimulated anchorage independent growth. However, when the IGF-IR targeted therapies were combined with SASP, IGF-I stimulated colony formation was completely (huEM164) or partially (AEW-541) inhibited in the MCF-7 cells, which was reversed by treating cells with NAC (Figure 6C). Notably, SASP enhanced the growth inhibition of anti-IGF-IR drugs at lower concentrations of these anti-IGF drugs than normally required (normally 20 μg/ml huEM164, 0.3 μM AEW-541) for maximal inhibition of signaling and growth (24). Similar results were observed by using BSO instead of SASP (Figure S8 C). Thus, the biological effects of IGF-IR inhibition could be enhanced by disrupting xCT effects while using lower doses of the anti-IGF-IR drugs.

## Discussion

It is well known that cellular ROS causes genome instability and mutation to stimulate tumorigenesis and increase resistance to therapy. Our data revealed that IGF-I signaling increases $xC^-$ transporter expression and function in IRS-1 activated ER positive to affect cellular redox status and promote proliferation. We also further found that stimulation MCF-7 cells with IGF-II or insulin both induced xCT mRNA expression (Figure S7) implying a similar role for insulin receptor acting through IRS-1. These data imply that ER positive breast cancer cells require activated IRS-1 signaling to overcome oxidative stress. In contrast, the high basal levels of xCT in ER-independent breast cancer cells might have

mobilized a set of ROS adaptive mechanisms independent of the growth factor/IRS-1 signaling.

It has been recently reported that CD44 variant stabilizes cell surface xCT expression (15). Given that MDA-MB-231 cells are CD44 positive and MCF-7 cells are CD44 negative (32), we confirmed that the basal expression and function of xCT was significantly higher in MDA-MB-231 cells than in MCF-7 cells (Figure 1B right panel, 4A). MCF-7 cells expressed little amount of CD44 variant, and none of the IGF ligands (IGF-I, IGF-II, insulin) regulated CD44v mRNA expression (Figure S7) indicating that the xCT regulation of IGF-I might be independent of CD44 variant.

Although in our study the expression and function of $xC^-$ is not regulated by IGF-I in MDA-MB-231 cells, we still found that low concentration of SASP (0.1 mM) treatment depleted the cellular GSH level; genetically downregulation of xCT or SASP treatment also decreased the basal proliferation and migration in MDA-MB-231 cells (data not shown). A recent study showed that $xC^-$ transporters are commonly expressed in triple negative breast cancer cells. Targeting $xC^-$transporters might yield another therapeutic opportunity for the triple negative breast cancers as well (33). Our data also suggest that $xC^-$ targeting could have a role in ER-positive breast cancer cells.

We observed that down-regulation of IRS-1 by siRNA resulted in a significant increase of basal xCT protein expression (Figure 3A lower right panel). Consistently, in our experiments, we also observed that the basal xCT expression in MCF-7L TamR was higher than that in MCF-7L parental cells (Figure 1D lower right panel). We further examined the xCT protein expression in T47D-YA and T47D-YA-IRS-1 cells and found that T47D-YA cells expressed significantly more xCT protein than T47D-YA-IRS-1 cells did (data not shown). In patient specimens, ER expression tended to negatively correlated with xCT expression while positively correlated with IRS-1 expression in TCGA breast cancer database (data not shown). Given the development of new anti-IRS-1 targeted therapies (34), our data suggest that IRS-1 targeting might have adverse effects on ROS status. Further investigation is needed to understand the potential role of IRS-1 protein expression in regulating xCT expression levels.

In this study, we inhibited xCT function with SASP and also used the potent glutathione inhibitor BSO to examine the effects of GSH levels on breast cancer growth. (Figure S8). Both compounds were effective inhibitors highlighting the important role of glutathione in breast cancer cells.

Identification of predictive biomarkers to identify patient populations appropriate for treatment with targeted therapies would improve patient benefit. In addition, identification of key targets in a pathway could result in rational combination therapies. While anti-IGF-IR therapy has not yet proven to be of benefit in unselected patients, it is possible that biomarkers, such as IRS-1, might be used to identify IGF-IR driven tumors. Our findings also suggested that $xC^-$ transporter could be a promising biomarker in predicting prognosis in breast cancer patients. While we focused on ER positive tumors, the recent data suggest a role for this protein in basal breast cancer (33).

Indeed, recently a promising novel positron emission tomography tracer, (4S)-4-(3-[18F]fluoropropyl)-L-glutamate, specifically for imaging $xC^-$ transporter activity has been proved to have high cancer detection rate in rodents (35) and in clinic trial of patients with non-small cell lung cancer and metastasis or invasive breast cancer (36). This imaging technique also would offer clinicians a convenient way to monitor malignant cells' adaptation to oxidative stress *in vivo*. Besides, our findings also implied that co-targeting IGF-IR with $xC^-$ transporter might reduce the dosage of anti-IGF-IR agents and attenuate potential side effects. Coupling chemotherapy or radiotherapy with $xC^-$ inhibitor might also achieve synergic therapeutic effect.

In conclusion, our study reveals that IGF-I regulates oxidative stress and thereby promotes proliferation by stimulating $xC^-$ transporter function in an IRS-1 dependent mechanism. $xC^-$ transporter expression level could be a promising biomarker to indicate tumor metabolic status to oxidative stress. $xC^-$ transporter could be also be a target to enhance anti-IGF-IR therapy, chemotherapy, and radiotherapy in multiple subtypes of breast cancer.

## Supplementary Material

Refer to Web version on PubMed Central for supplementary material.

## Acknowledgments

We would like to acknowledge the assistance of the Flow Cytometry shared resource of the Masonic Cancer Center (P30 CA077598). Work was also supported by R01CA74285 and the Komen for the Cure grant (SAC 110039)

This study was supported by R01CA74285 to D.Y., and the Komen for the Cure grant (SAC 110039) to D.Y. and P30 CA077598.

## Reference

1. Sachdev D, Yee D. The IGF system and breast cancer. Endocr Relat Cancer. 2001; 8:197–209. [PubMed: 11566611]
2. Pollak M. The insulin and insulin-like growth factor receptor family in neoplasia: an update. Nat Rev Cancer. 2012; 12:159–69. [PubMed: 22337149]
3. Taniguchi CM, Emanuelli B, Kahn CR. Critical nodes in signalling pathways: insights into insulin action. Nature reviews Molecular cell biology. 2006; 7:85–96.
4. Jackson JG, White MF, Yee D. Insulin receptor substrate-1 is the predominant signaling molecule activated by insulin-like growth factor-I, insulin, and interleukin-4 in estrogen receptor-positive human breast cancer cells. J Biol Chem. 1998; 273:9994–10003. [PubMed: 9545345]
5. Byron SA, Horwitz KB, Richer JK, Lange CA, Zhang X, Yee D. Insulin receptor substrates mediate distinct biological responses to insulin-like growth factor receptor activation in breast cancer cells. Br J Cancer. 2006; 95:1220–8. [PubMed: 17043687]
6. Jackson JG, Zhang X, Yoneda T, Yee D. Regulation of breast cancer cell motility by insulin receptor substrate-2 (IRS-2) in metastatic variants of human breast cancer cell lines. Oncogene. 2001; 20:7318–25. [PubMed: 11704861]
7. Kaufman PA, Ferrero JM, Bourgeois H, Kennecke H, De Boer R, Jacot W, et al. A Randomized, Double-Blind, Placebo-Controlled, Phase 2 Study of AMG 479 With Exemestane (E) or Fulvestrant (F) in Postmenopausal Women With Hormone-Receptor Positive (HR+) Metastatic (M) or Locally Advanced (LA) Breast Cancer (BC). Cancer research. 2010:70.
8. Yang Y, Yee D. Targeting Insulin and Insulin-Like Growth Factor Signaling in Breast Cancer. J Mammary Gland Biol Neoplasia. 2012

9. Yee D. Insulin-like growth factor receptor inhibitors: baby or the bathwater? Journal of the National Cancer Institute. 2012; 104:975–81. [PubMed: 22761272]
10. Lo M, Wang YZ, Gout PW. The x(c)- cystine/glutamate antiporter: a potential target for therapy of cancer and other diseases. J Cell Physiol. 2008; 215:593–602. [PubMed: 18181196]
11. Vaughn AE, Deshmukh M. Glucose metabolism inhibits apoptosis in neurons and cancer cells by redox inactivation of cytochrome c. Nature cell biology. 2008; 10:1477–83.
12. Sartorius CA, Groshong SD, Miller LA, Powell RL, Tung L, Takimoto GS, et al. New T47D breast cancer cell lines for the independent study of progesterone B- and A-receptors: only antiprogestin-occupied B-receptors are switched to transcriptional agonists by cAMP. Cancer research. 1994; 54:3868–77. [PubMed: 8033109]
13. Trachootham D, Alexandre J, Huang P. Targeting cancer cells by ROS-mediated mechanisms: a radical therapeutic approach? Nature reviews Drug discovery. 2009; 8:579–91.
14. Cairns RA, Harris IS, Mak TW. Regulation of cancer cell metabolism. Nat Rev Cancer. 2011; 11:85–95. [PubMed: 21258394]
15. Ishimoto T, Nagano O, Yae T, Tamada M, Motohara T, Oshima H, et al. CD44 variant regulates redox status in cancer cells by stabilizing the xCT subunit of system xc(−) and thereby promotes tumor growth. Cancer Cell. 2011; 19:387–400. [PubMed: 21397861]
16. Trachootham D, Lu W, Ogasawara MA, Nilsa RD, Huang P. Redox regulation of cell survival. Antioxidants & redox signaling. 2008; 10:1343–74. [PubMed: 18522489]
17. Schneider BL, Kulesz-Martin M. Destructive cycles: the role of genomic instability and adaptation in carcinogenesis. Carcinogenesis. 2004; 25:2033–44. [PubMed: 15180945]
18. Chen EI, Hewel J, Krueger JS, Tiraby C, Weber MR, Kralli A, et al. Adaptation of energy metabolism in breast cancer brain metastases. Cancer research. 2007; 67:1472–86. [PubMed: 17308085]
19. Sullivan R, Graham CH. Chemosensitization of cancer by nitric oxide. Current pharmaceutical design. 2008; 14:1113–23. [PubMed: 18473858]
20. Sato H, Shiiya A, Kimata M, Maebara K, Tamba M, Sakakura Y, et al. Redox imbalance in cystine/glutamate transporter-deficient mice. J Biol Chem. 2005; 280:37423–9. [PubMed: 16144837]
21. Chen RS, Song YM, Zhou ZY, Tong T, Li Y, Fu M, et al. Disruption of xCT inhibits cancer cell metastasis via the caveolin-1/beta-catenin pathway. Oncogene. 2009; 28:599–609. [PubMed: 19015640]
22. Huang Y, Dai Z, Barbacioru C, Sadee W. Cystine-glutamate transporter SLC7A11 in cancer chemosensitivity and chemoresistance. Cancer Res. 2005; 65:7446–54. [PubMed: 16103098]
23. Pham AN, Blower PE, Alvarado O, Ravula R, Gout PW, Huang Y. Pharmacogenomic approach reveals a role for the x(c)- cystine/glutamate antiporter in growth and celastrol resistance of glioma cell lines. The Journal of pharmacology and experimental therapeutics. 2010; 332:949–58. [PubMed: 20007406]
24. Fagan DH, Uselman RR, Sachdev D, Yee D. Acquired resistance to tamoxifen is associated with loss of the type I insulin-like growth factor receptor: implications for breast cancer treatment. Cancer Res. 2012; 72:3372–80. [PubMed: 22573715]
25. www.oncomine.org
26. Lee AV, Jackson JG, Gooch JL, Hilsenbeck SG, Coronado-Heinsohn E, Osborne CK, et al. Enhancement of insulin-like growth factor signaling in human breast cancer: estrogen regulation of insulin receptor substrate-1 expression in vitro and in vivo. Mol Endocrinol. 1999; 13:787–96. [PubMed: 10319328]
27. Gyorffy B, Lanczky A, Eklund AC, Denkert C, Budczies J, Li Q, et al. An online survival analysis tool to rapidly assess the effect of 22,277 genes on breast cancer prognosis using microarray data of 1,809 patients. Breast cancer research and treatment. 2010; 123:725–31. [PubMed: 20020197]
28. Griffith OW, Meister A. Potent and specific inhibition of glutathione synthesis by buthionine sulfoximine (S-n-butyl homocysteine sulfoximine). J Biol Chem. 1979; 254:7558–60. [PubMed: 38242]

29. Leach JK, Van Tuyle G, Lin PS, Schmidt-Ullrich R, Mikkelsen RB. Ionizing radiation-induced, mitochondria-dependent generation of reactive oxygen/nitrogen. Cancer research. 2001; 61:3894–901. [PubMed: 11358802]

30. Zafarullah M, Li WQ, Sylvester J, Ahmad M. Molecular mechanisms of N-acetylcysteine actions. Cellular and molecular life sciences : CMLS. 2003; 60:6–20. [PubMed: 12613655]

31. Wiemer EA. Stressed tumor cell, chemosensitized cancer. Nature medicine. 2011; 17:1552–4.

32. Sheridan C, Kishimoto H, Fuchs RK, Mehrotra S, Bhat-Nakshatri P, Turner CH, et al. CD44+/CD24− breast cancer cells exhibit enhanced invasive properties: an early step necessary for metastasis. Breast cancer research : BCR. 2006; 8:R59. [PubMed: 17062128]

33. Timmerman LA, Holton T, Yuneva M, Louie RJ, Padro M, Daemen A, et al. Glutamine Sensitivity Analysis Identifies the xCT Antiporter as a Common Triple-Negative Breast Tumor Therapeutic Target. Cancer cell. 2013

34. Reuveni H, Flashner-Abramson E, Steiner L, Makedonski K, Song R, Shir A, et al. Therapeutic Destruction of Insulin Receptor Substrates for Cancer Treatment. Cancer Res. 2013

35. Koglin N, Mueller A, Berndt M, Schmitt-Willich H, Toschi L, Stephens AW, et al. Specific PET imaging of xC- transporter activity using a (1)(8)F-labeled glutamate derivative reveals a dominant pathway in tumor metabolism. Clinical cancer research : an official journal of the American Association for Cancer Research. 2011; 17:6000–11. [PubMed: 21750203]

36. Baek S, Choi CM, Ahn SH, Lee JW, Gong G, Ryu JS, et al. Exploratory clinical trial of (4S)-4-(3-[18F]fluoropropyl)-L-glutamate for imaging xC- transporter using positron emission tomography in patients with non-small cell lung or breast cancer. Clinical cancer research : an official journal of the American Association for Cancer Research. 2012; 18:5427–37. [PubMed: 22893629]

## Precis

Findings suggest that targeting a cell surface amino acid transporter may heighten the therapeutic efficacy of anti-IGFl receptor inhibitors, which may be broadly useful in treating various solid tumors.

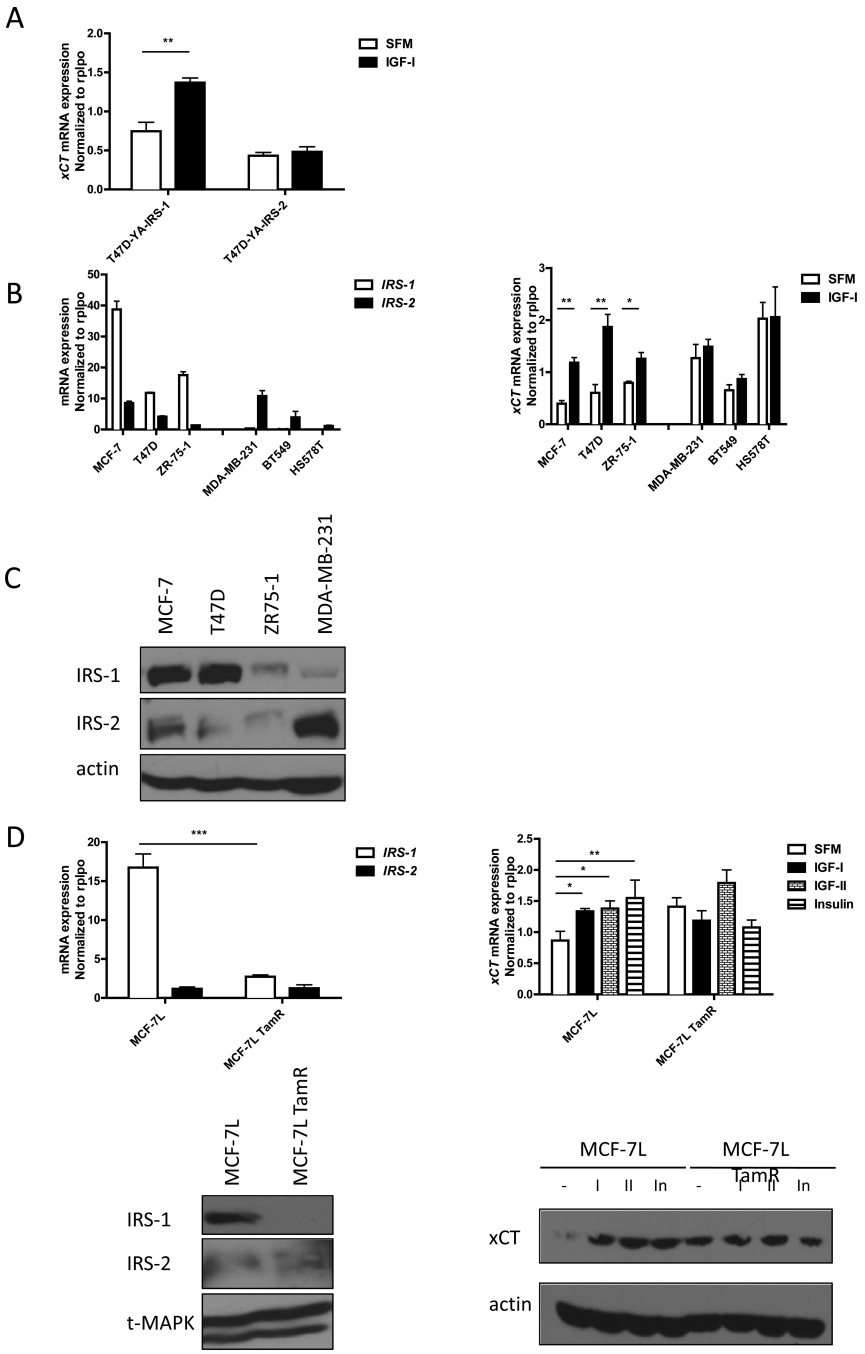


**Figure 1. IGF-I induced *xCT* mRNA expression in an IRS-1 dependent manner in breast cancer cell lines**

**(A)** T47D-YA-IRS-1 and Y47D-YA-IRS-2 cells were grown in SFM for 24 h. After 4 h of IGF-I (5 nM) exposure, mRNA was isolated and analyzed by qRT-PCR. mRNA expression of *xCT* was normalized to the *RPLPO* housekeeper gene. **(B)** Left: mRNA expression of IRS-1 and IRS-2 in ER positive cell lines: MCF-7, T47D, and ZR-75-1; ER negative breast cancer cell lines: MDA-MB-231, BT549, and HS578T were analyzed by qRT-PCR. Right: mRNA expression of *xCT* in SFM or 4 hours after IGF-I exposure was analyzed by qRT-PCR. **(C)** Immunoblot analysis of the expression levels of IRS-1 and IRS-2 in indicated breast cancer cell lines. **(D)** mRNA expression of IRS-1 and IRS-2 in full growth media were analyzed in MCF-7L and MCF-7L TamR cells (upper panels left). Right: mRNA expression of *xCT* in MCF-7L and MCF-7L TamR cells after 4 h of

IGF-I (5 nM), IGF-II (10 nM), or insulin (10 nM) exposure. Lower panels right: IRS-1 and IRS-2 protein expression in MCF-7L and MCF-7L TamR cells in full growth media condition. xCT expression in MCF-7L and MCF-7L TamR after 24 h of ligand stimulation was analyzed by immunoblot (right panel). Data are presented as mean ± standard error of the mean (SEM); all results are representative of three independent replicates.

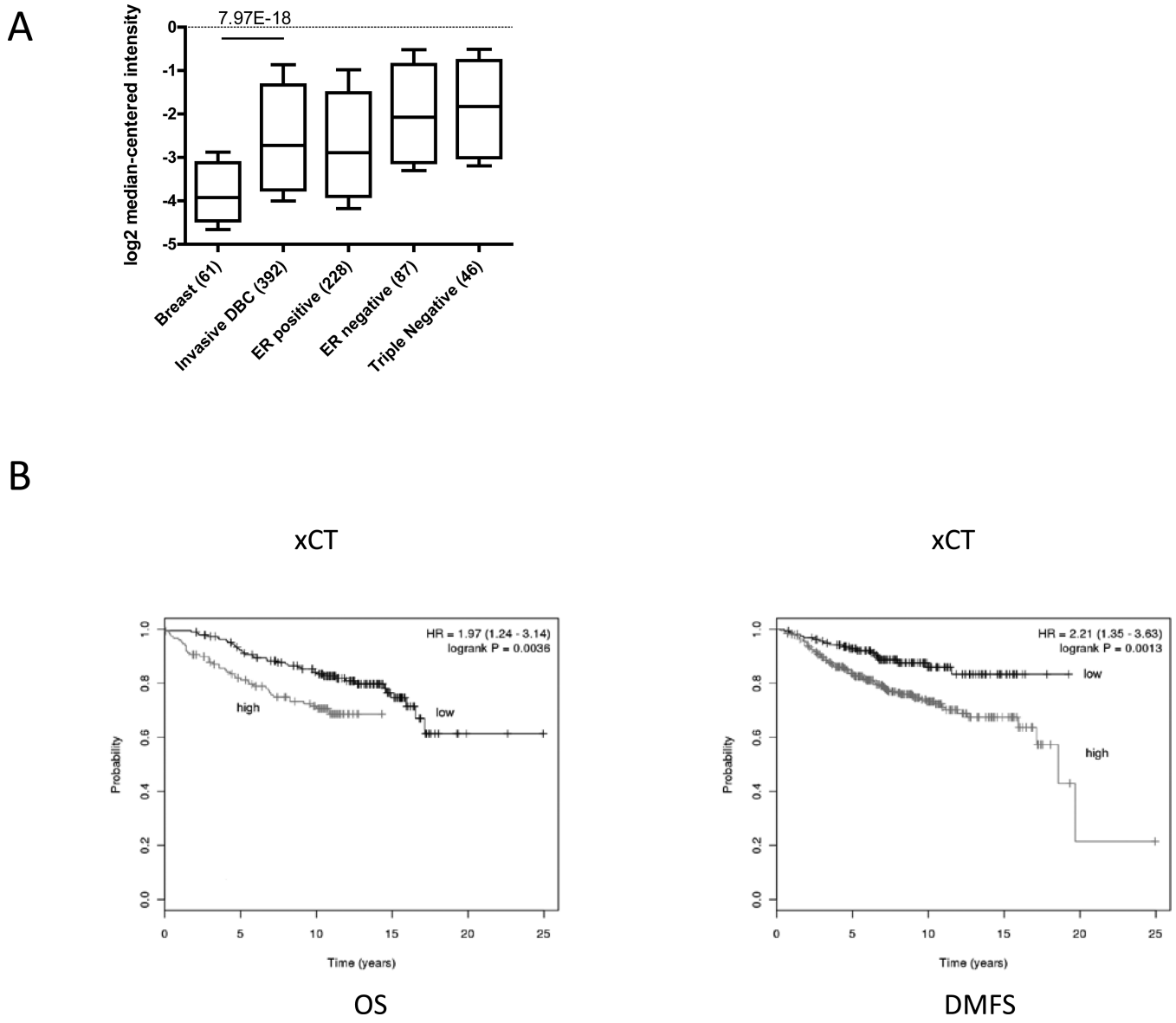


**Figure 2. xCT is overexpressed breast tumor and associated with poor prognosis in ER positive breast cancer**

**(A)** Oncomine output data was sorted to isolate specified associations as indicated and reported as the mRNA copy number unit expression values for normal breast, invasive ductal breast carcinoma, ER positive breast carcinoma, ER negative breast carcinoma, and triple negative breast carcinoma samples using box-and-whiskers plots (whiskers: 90/10 percentiles, box: 75/25 percentiles, line: median of all samples). **(B)** Kaplan-Meier plots of OS (left) and DMFS (right) of ER positive breast cancer patients with high or low expression of xCT. Data obtained from the Kaplan-Meier plotter database.

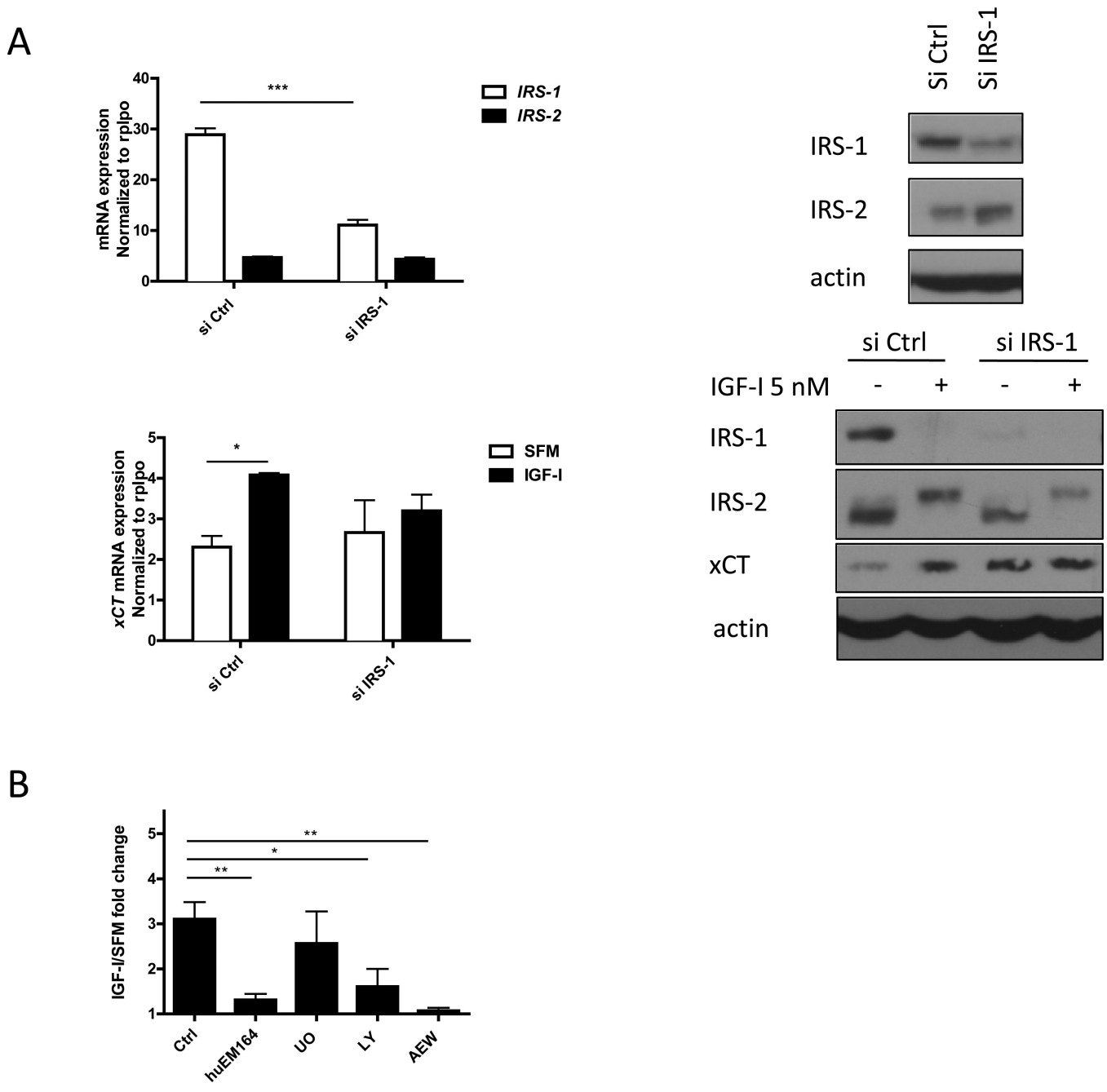


**Figure 3. IGF-I induced xCT mRNA and protein expression specifically through IRS-1 and via PI3K dependent pathway in MCF-7 cells**

**(A)** MCF-7 cells were transfected with either 30 nM of control or IRS-1 siRNA for 48h. siRNA knockdown efficiency was determined by both qRT-PCR (upper left) and immunoblot analysis (upper right). Cells then were grown in SFM for 24 h followed by IGF-I (5 nM) stimulation for 4 h for mRNA measurement (lower left) and 24 h for protein detection (lower right). **(B)** MCF-7 cells were grown in SFM for 24 h and pretreated with huEM164 (20 μg/ml) for 24 h; pretreated with 10 UO126 (UO; 10 μM), LY294002 (LY; 10 μM), or NVP AEW-541 (AEW; 0.5 μM) for 30 min. Cells were then treated with IGF-I for 4 h for qRT-PCR. Data are mean ± SEM; all qRT-PCR results are representative of at least three independent triplicates-experiments.

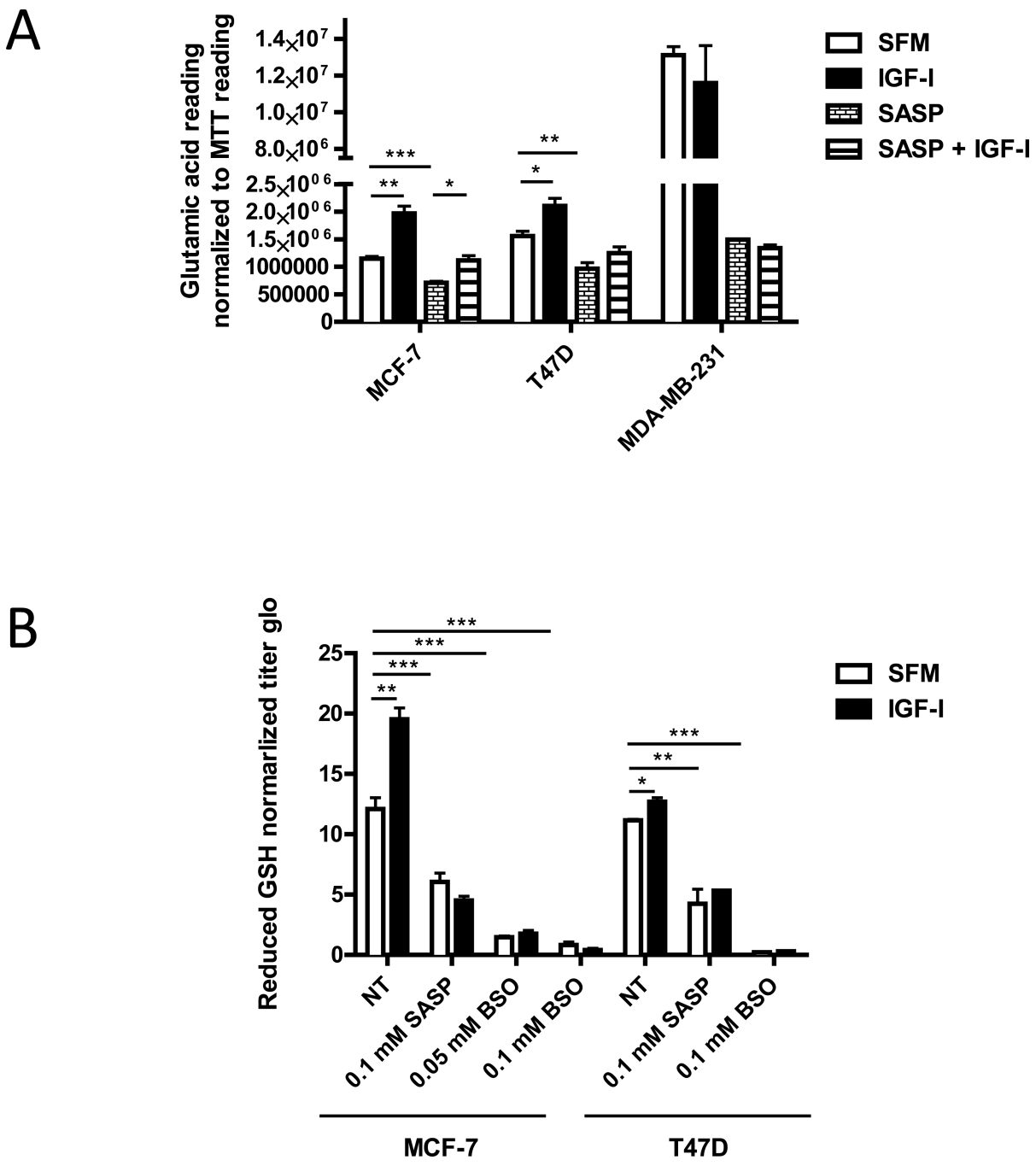


**Figure 4. IGF-I stimulated xC− transporter function in ER positive breast cancer cells**

Cells were pretreated with SASP (0.1 mM) for 48 h, BSO (0.05 or 0.1 mM) for 24 h. **(A)** MCF-7, T47D, and MDA-MB-231 cells were grown in SFM for 24 h then treated with indicated treatments with or without IGF-I (5nM) for another 24 h. Culture media glutamic acid levels were analyzed and readings were normalized to MTT reading. **(B)** MCF-7 and T47D cells were grown in SFM for 24 h then treated with indicated treatments with or without IGF-I (5nM) for another 24 h. Intracellular reduced GSH concentration was determined as described. Data are mean ± SEM; all results are representative of three independent replicates.

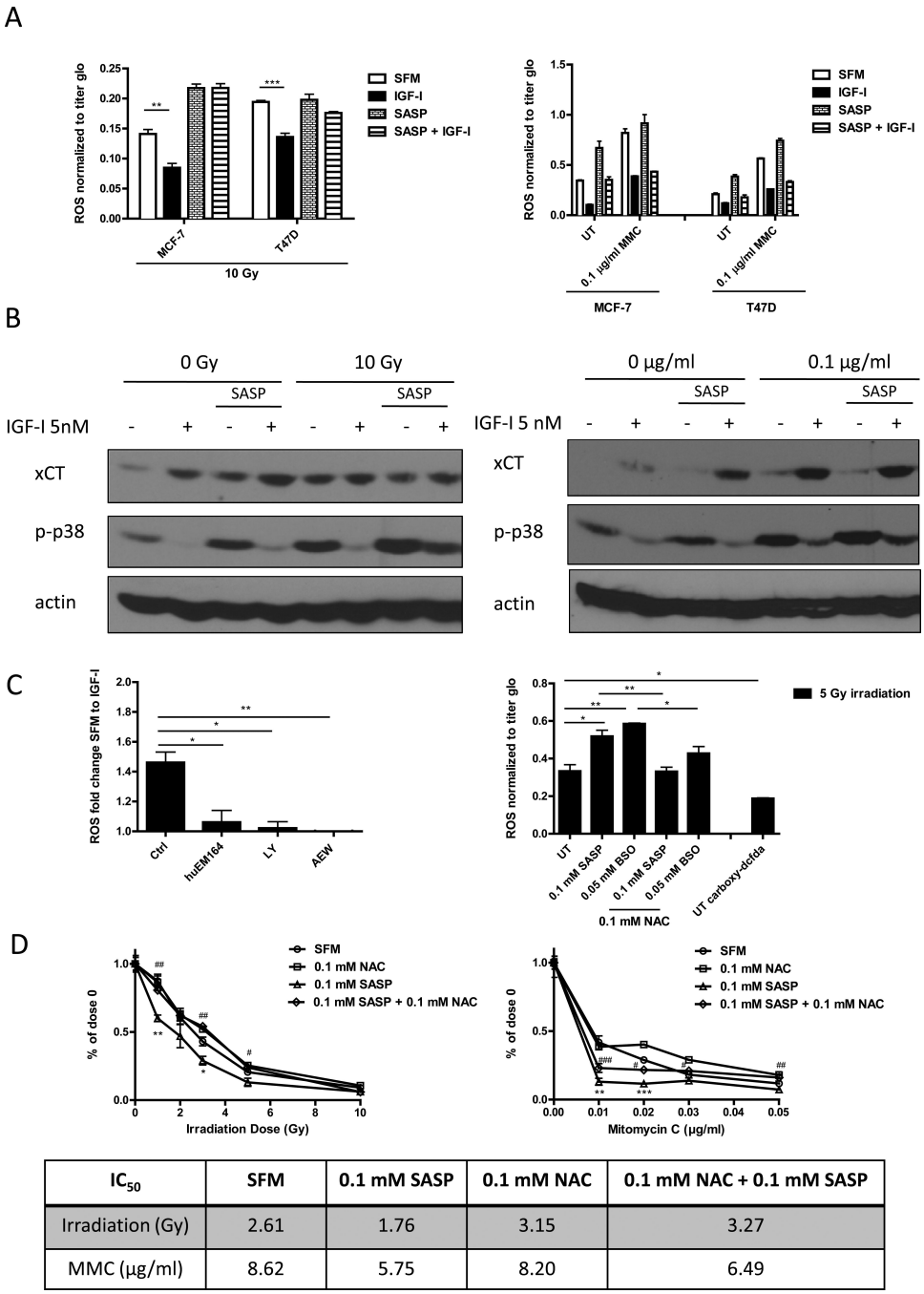


| $IC_{50}$ | SFM | 0.1 mM SASP | 0.1 mM NAC | 0.1 mM NAC + 0.1 mM SASP |
|---|---|---|---|---|
| Irradiation (Gy) | 2.61 | 1.76 | 3.15 | 3.27 |
| MMC (μg/ml) | 8.62 | 5.75 | 8.20 | 6.49 |

**Figure 5. IGF-I regulated intracellular ROS level via xC⁻ transporter and through PI3K dependent pathway in ER positive breast cancer cells**

**(A)** MCF-7 and T47D cells were pretreated with or without SASP (0.1 mM) for 48 h, grown in SFM for 24h, treated with IGF-I (5 nM) for another 24h, and then irradiated (10 Gy, left panel) or treated with mitomycin C treatment (1 μg/ml for ROS assay; 0.1 μg/ml for immunoblot) for 3 days (right panel). Intracellular ROS levels were measured as described. **(B)** Cellular phospho-$p38^{MAPK}$ level was determined by immunoblot. **(C)** MCF-7 cells were grown in SFM, pretreated huEM164 (20 μg/ml), LY294002 (10 μM), or NVP AEW-541 (0.5 μM) (Left panel). MCF-7 cells were pretreated with indicated dosage of SASP, BSO, or NAC. Acute ROS were induced by 5 gy irradiation. MCF-7 cells incubated with ROS insensitive probe carboxy-

DCFDA (0.1 mM) was presented as assay control (Right panel). Cellular ROS levels were determined as described. **(D)** MCF-7 cells were treated with indicated treatments in soft agar. After 24h of synchronization in SFM condition, cells were either irradiated or treated with mitomycin C. Colony formation was assessed after 14 days. Survival rate curve was determined by normalizing colony number of each treatment to its own no treatment control. Statistically significant differences are noted (* or # $p<0.5$, ** or ## $p<0.01$, *** or ### $p<0.001$). $IC_{50}$ values were shown in the table. Data are mean ± SEM; all results are representative of three independent replicates.

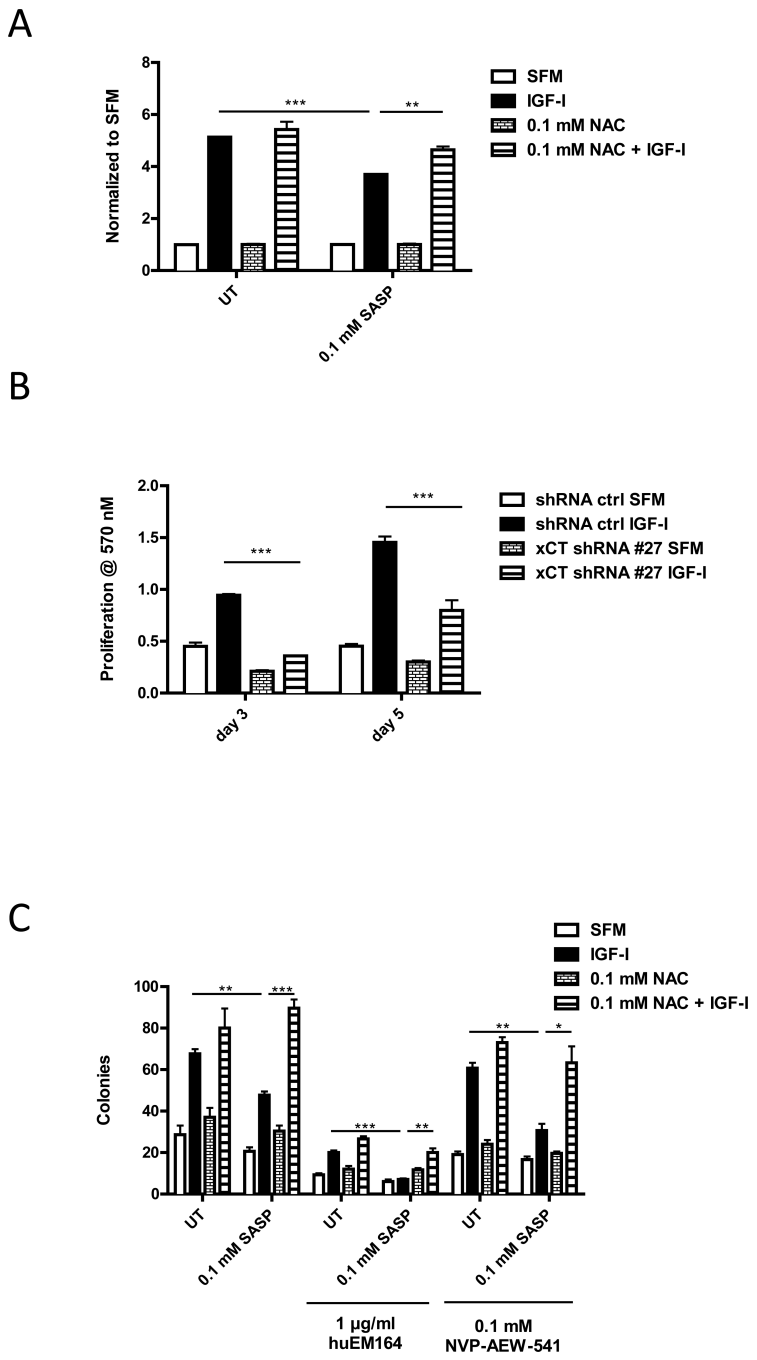


**Figure 6. Disruption of xC⁻ transporter function resulted in partial suppression in IGF-I-induced cell proliferation and sensitized cells to IGF-IR inhibitors**

**(A)** MCF-7 cells were first pretreated with SASP (0.1 mM) for 48 h or NAC (0.1 mM) for 24 h in SFM and then treated with IGF-I (5 nM) for 5 days. Cell viability was determined by performing MTT assay. **(B)** MCF-7 cells were infected by either scrambled shRNA or xCT specific shRNA to generate stable xCT down-regulation clone. Cells were grown in SFM for 24h then treated with IGF-I (5 nM) for 3 days or 5 days. Cell monolayer growth was measured by MTT assay. **(C)** MCF-7 cells were treated with indicated treatment combinations. Anchorage independent growth was determined after 14 days. Data are mean ± SEM; all results are representative of three independent replicates.

## Table 1

Cell cycle phase percentages were determined by flow cytometry.

| Cell cycle phase (%) | SFM | IGF-I | SASP | SASP + IGFI | NAC+ SASP | NAC + SASP + IGFI |
|---|---|---|---|---|---|---|
| G0/G1 | 74.84 | 45.16 | 72.64 | 62.81 | 74.77 | 47.06 |
| S | 8.42 | 46.88 | 8.81 | 23.26 | 8.65 | 41.94 |
| G2/M | 15.99 | 7.28 | 17.62 | 13.21 | 14.95 | 10.64 |